

TECHNICAL REPORT ARCCB-TR-01017

**HIGH-RATE SPUTTER-DEPOSITED
TANTALUM COATINGS ON A STEEL LINER
FOR WEAR AND EROSION MITIGATION**

**S. L. LEE
J. COX
D. WINDOVER**

**M. AUDINO
D. W. MATSON
E. D. McCLANAHAN**

AUGUST 2001



**US ARMY ARMAMENT RESEARCH,
DEVELOPMENT AND ENGINEERING CENTER
CLOSE COMBAT ARMAMENTS CENTER
BENÉT LABORATORIES
WATERVLIET, N.Y. 12189-4050**



APPROVED FOR PUBLIC RELEASE; DISTRIBUTION UNLIMITED

20010905 062

DISCLAIMER

The findings in this report are not to be construed as an official Department of the Army position unless so designated by other authorized documents.

The use of trade name(s) and/or manufacturer(s) does not constitute an official endorsement or approval.

DESTRUCTION NOTICE

For classified documents, follow the procedures in DoD 5200.22-M, Industrial Security Manual, Section II-19, or DoD 5200.1-R, Information Security Program Regulation, Chapter IX.

For unclassified, limited documents, destroy by any method that will prevent disclosure of contents or reconstruction of the document.

For unclassified, unlimited documents, destroy when the report is no longer needed. Do not return it to the originator.

REPORT DOCUMENTATION PAGE			Form Approved OMB No. 0704-0188	
Public reporting burden for this collection of information is estimated to average 1 hour per response, including the time for reviewing instructions, searching existing data sources, gathering and maintaining the data needed, and completing and reviewing the collection of information. Send comments regarding this burden estimate or any other aspect of this collection of information, including suggestions for reducing this burden, to Washington Headquarters Services, Directorate for Information Operations and Reports, 1215 Jefferson Davis Highway, Suite 1204, Arlington, VA 22202-4302, and to the Office of Management and Budget, Paperwork Reduction Project (0704-0188), Washington, DC 20503.				
1. AGENCY USE ONLY (Leave blank)		2. REPORT DATE August 2001	3. REPORT TYPE AND DATES COVERED Final	
4. TITLE AND SUBTITLE HIGH-RATE SPUTTER-DEPOSITED TANTALUM COATINGS ON A STEEL LINER FOR WEAR AND EROSION MITIGATION			5. FUNDING NUMBERS AMCMS No. 7780.45.E251.200	
6. AUTHOR(S) S.L. Lee, J. Cox, D. Windover (Benet and RPI, Troy, NY), M. Audino, D.W. Matson (Pacific Northwest National Laboratory, Richland, WA), and E.D. McClanahan (Pacific Northwest National Laboratory)				
7. PERFORMING ORGANIZATION NAME(S) AND ADDRESS(ES) U.S. Army ARDEC Benet Laboratories, AMSTA-AR-CCB-O Watervliet, NY 12189-4050			8. PERFORMING ORGANIZATION REPORT NUMBER ARCCB-TR-01017	
9. SPONSORING / MONITORING AGENCY NAME(S) AND ADDRESS(ES) U.S. Army ARDEC Close Combat Armaments Center Picatinny Arsenal, NJ 07806-5000			10. SPONSORING / MONITORING AGENCY REPORT NUMBER	
11. SUPPLEMENTARY NOTES Presented at the International Conference on Metallurgical Coatings and Thin Films 2001, San Diego, CA, 30 April - 4 May 2001. To be published in <i>Surface and Coatings Technology</i> .				
12a. DISTRIBUTION / AVAILABILITY STATEMENT Approved for public release; distribution unlimited.			12b. DISTRIBUTION CODE	
13. ABSTRACT (Maximum 200 words) A prototype, rifled steel liner of 20-mm inside diameter was coated with ~50 to 125 μm tantalum at ~22.6 $\mu\text{m}/\text{hour}$ in krypton gas using a triode-sputter system. It was test fired with 1500 rounds for the mitigation of high-temperature and pressure wear and erosion. Growth surface analysis showed predominately α -phase and minimal β -phase surface tantalum. Area detector images showed near random, slight preferred (211) crystalline orientation. X-ray diffraction revealed a thin layer of surface zinc oxide and copper firing debris on the coating surface. Compressive surface residual stress peaked near the center of the tube. Photomicrograph metallurgical examination showed general good adhesion in major parts of the bulk coatings, along with a thin layer of β -phase nucleation, and α -phase or mixed α - and β -phase grain growth. There was excellent behavior in soft and ductile α -tantalum areas, but cracking and disbonding occurred in β -tantalum areas. Coating liftoff and coating loss occurred most frequently in land/groove transition and land areas, less in groove areas. Near the breech end where no coating was sputtered, the steel substrate suffered extensive cracking and environmentally-assisted heat damages.				
14. SUBJECT TERMS Sputtering, Triode Sputtering, Tantalum, Thick Coating, Refractory Coating, Phase, Residual Stress, Anisotropy			15. NUMBER OF PAGES 24	
			16. PRICE CODE	
17. SECURITY CLASSIFICATION OF REPORT UNCLASSIFIED	18. SECURITY CLASSIFICATION OF THIS PAGE UNCLASSIFIED	19. SECURITY CLASSIFICATION OF ABSTRACT UNCLASSIFIED	20. LIMITATION OF ABSTRACT UL	

TABLE OF CONTENTS

	<u>Page</u>
ACKNOWLEDGEMENTS	iii
INTRODUCTION.....	1
SPUTTERING EXPERIMENTAL METHOD.....	2
ANALYSIS	2
X-Ray Diffraction Surface Phase and Preferred Orientation	3
Surface Texture and Anisotropy	4
Surface Chemical Composition.....	4
Hardness	4
Residual Stress	4
Photomicrograph Analysis	5
DISCUSSION	6
Tantalum Phases.....	6
Residual Stress	7
Microstructure	7
Surface Firing Debris	7
CONCLUSIONS	7
REFERENCES.....	9

TABLES

1.	Summary of Sputtered 20-mm Liner After 1500 Rounds of Firing Test.....	3
----	--	---

LIST OF ILLUSTRATIONS

1a.	Liner configuration from breech to muzzle end.....	11
1b.	Land and groove geometry in a rifled tube	11
1c.	Triode-sputter apparatus at Pacific Northwest National Laboratory	12
2a.	Growth surface x-ray diffraction from breech to muzzle end (sections 1 through 4), showing surface α -phase tantalum, and oxide and copper firing debris	13

2b.	Grazing incidence x-ray diffraction at $\omega = 5^\circ$ and $\omega = 2^\circ$ compared to conventional x-ray diffraction, demonstrating that the observed zinc oxide and copper are on the surface of sputtered tantalum coating	14
2c.	Growth surface x-ray diffraction after etching to remove surface firing debris, showing all α -phase tantalum, residual zinc oxide and copper, and minor relative intensity change due to differential etching	14
3.	Two-dimensional area detector images of groove areas of the four sections after etching	15
4a.	Photomicrograph of specimen cut from section #1 of the liner	16
4b.	Photomicrograph of specimen cut from section #2 of the liner	16
4c.	Photomicrograph of specimen cut from section #3 of the liner	17
4d.	Photomicrograph of specimen cut from section #4 of the liner	17
4e.	Single-phase α -tantalum with good cohesion and adhesion to the 4340 steel substrate	18
4f.	Coating with β -phase tantalum nucleation and mixed α - and β -growth, showing horizontal and vertical cracks in the β -tantalum region	18
5a.	Land/groove area of sputtered tantalum coating on steel after firing 1500 rounds.....	19
5b.	Typical cracks in the land/groove transition area, showing a piece of copper on the left arm of the land/groove transition area	19
5c.	Coating loss in the land/groove transition area, revealing large crack near tantalum/steel interface	20
6a.	Cracks in bare steel in the direction of high-friction sliding due to projectile motion, in areas with no sputtered tantalum (unetched)	20
6b.	Environmental-assisted heat damages in steel forming white and gray layers in areas with no sputtered tantalum (etched).....	21

ACKNOWLEDGEMENTS

The authors wish to thank the Strategic Environmental Research and Development Program (SERDP)-Green Gun Barrel Project for funding this work. The authors also wish to thank Steven Liss, Steve Kelley, and Benjamin Wong of ARDEC for information on the chemical composition of the projectiles; Greg Vigilante, Chris Mulligan, Tom Sage, and Chris Rickard for specimen preparation and work on the photomicrographs.

INTRODUCTION

Chromium, electrochemically deposited from aqueous solution, significantly improves wear lifetime in high-temperature pressure vessels. However, Cr(VI), formed in the chromium acid solution during the electrolytic deposition process, is hazardous and toxic waste disposal is a problem. To prevent high-temperature and pressure wear and erosion of gun bores, environmentally clean sputter deposition of refractory metals, such as tantalum, is being considered to replace electrolytic chromium.

High-temperature coating materials, such as tantalum, tungsten, molybdenum, tantalum-tungsten, tantalum-chromium, oxides, and carbides have been considered for gun bore applications (refs 1-3). A cylindrical magnetron sputter-deposition system and process are being developed for the deposition of protective coatings onto the interior bore surface of cylinders with large length-to-diameter ratios (ref 4). Tantalum is selected because bulk tantalum (body-centered-cubic phase) possesses the following excellent physical properties:

- Melting point temperature of 2996°C
- Elastic modulus similar to steel
- Good ductility
- Low thermal conductivity
- Chemical resistance to aggressive propellant gases

A number of experimental investigations have been undertaken to evaluate tantalum for wear and erosion protection. Cullinan *et al.* (ref 5)] and Ahmad *et al.* (ref 6) investigated the deposition of tantalum and tantalum-chromium (chromium to improve hardness) onto 20-mm liners using a fused electrolyte with eutectic mixtures of alkali metal fluorides and K_2TaF_7 or K_2NbF_7 salts. Lee *et al.* (ref 7) studied the tantalum liner produced in fused salt at 800°C after firing 5034 rounds and found excellent adhesion and cohesion, uniform, randomly-oriented α -phase tantalum, surface tantalum oxides, and swaging in tantalum. Cox *et al.* (ref 8) reported triode-sputter coating deposition onto smooth bores and rifled 20-mm and 120-mm bores at deposition temperatures under 500°C. Matson *et al.* (ref 9) deposited tantalum onto steel cylinders with and without a niobium interface layer, and Lee *et al.* (ref 10) studied phase, texture, and stress in the coating. Matson *et al.* (ref 11) further suggested that heavier sputtering gas species, higher substrate temperature, and sputter-cleaning procedures improve the phase and microstructure properties of sputtered tantalum for gun bore applications.

In this investigation, a type 4340 steel liner was sputter-deposited with 50 to 125 μm tantalum coating in krypton gas using a triode-sputtering system at Pacific Northwest National Laboratory. The outside diameter of the steel liner was coated with $\sim 200\text{-}\mu\text{m}$ electrolytic chromium for easy shrink fitting into an M61A1 tube. The tube assembly was subjected to 1500 rounds of firing at 150 rounds/minute. This report summarizes the analysis of the sputter coating and steel substrate after firing.

SPUTTERING EXPERIMENTAL METHOD

As shown in Figure 1a, the rifled 4340 steel tube was 92.4-mm long with 20-mm inside diameter. It had a 9.6-mm by 32.7-mm collar at the breech end. Four sections were marked to facilitate data acquisition and analysis. Figure 1b shows the geometry of land and groove areas of the rifled liner.

Figure 1c shows the triode-sputter apparatus, which was previously described (refs 9,11). The chamber lid of the apparatus acted as the anode. The center tantalum target was hollow for water-cooling. The central tantalum tube was coaxial with the steel substrate tube, and acted as the cathode. The tube was mounted breech end up/muzzle end down. A tungsten filament on the bottom acted as an auxiliary cathode to support the plasma. The system was pumped down to a chamber base pressure of 4.8×10^{-7} Torr, backfilled with 3.6 mTorr (0.48 pa) krypton (99.99%) gas. An ion etch of the substrate tube was performed at -100 V dc and 500 mA for 30 minutes, although no shutter or "junk catcher" was in place to remove potential surface contamination. During the sputter process, substrate voltage was -50 V, target voltage was -1500 V dc, and target current was 250 mA. Thermocouples showed a temperature gradient as follows: average temperature was $\sim 257^{\circ}\text{C}$ (bottom), $\sim 217^{\circ}\text{C}$ (center), and $\sim 312^{\circ}\text{C}$ (top).

Target weight loss was 6.9 grams, and substrate weight gain was 6.1 grams. An average deposition rate of $22.6 \mu\text{m}/\text{hour}$ was calculated using the 6.1 grams weight gain, the 2.75 hours total deposition time, and assuming tantalum density of $16.67 \text{ gm}/\text{cm}^3$. An average coating thickness of $82 \mu\text{m}$ was calculated from the deposition rate, assuming a uniform coating thickness throughout the tube.

ANALYSIS

An axial slit was cut from the liner to expose the bore surface. X-ray diffraction phase, preferred orientation, and residual stress analysis were performed at the middle of the four sections along the tube axis, approximately 12, 35, 58, and 81-mm from the breech end. Four axial specimens were dissected and numbered section 1 through section 4 from breech to muzzle for further analysis. A thin cross-sectional slice was cut from the muzzle end of the tube for analysis around the circumference. Muzzle-end data were reported at two opposite locations on the circumference (0° and 180°). Table 1 summarizes our x-ray diffraction and photomicrograph data.

Table 1. Summary of Sputtered 20-mm Liner After 1500 Rounds of Firing Test

Specimen	Axial Section 1	Axial Section 2	Axial Section 3	Axial Section 4	Muzzle End 0°	Muzzle End 180°
From Breech ^a	12-mm	35-mm	58-mm	81-mm	90-mm	90-mm
X-Ray Diffraction Phase	α (Random)	α (Random)	α (211)	α (Random)		
Thickness (μm)	52	51	45	42 to 45	32 to 47 ^b	93 to 145 ^b
Phase (%)	$\alpha + \beta$ (2%)	$\alpha + \beta$ (2%)	$\alpha + \beta$ (7%)	$\alpha + \beta$ (7%)	$\alpha + \beta$ (Greater)	α
Stress (MPa)	-545	-399	-267	-583	-792	

^a Distance from the breech end to the middle of the axial section.

^b Multiple measurements around the circumference, centered around 0° and 180°.

X-Ray Diffraction Surface Phase and Preferred Orientation

Figure 2a shows the x-ray diffraction growth surface scans of the four axial specimens. Data for the four sections were fairly consistent revealing predominately α -phase surface tantalum and concentrations of zinc oxide and copper firing debris. However, due to possible overlapping peaks, we do not rule out the existence of β -phase tantalum. Relative intensities of α -tantalum reflections compared to random powder revealed near-random, but slight preferred (211) crystalline orientation. Section 3 shows stronger (211) preferred orientation.

Figure 2b shows grazing incidence x-ray diffraction data of section 2 of the axial specimens. In conventional Bragg-Brentano scans, specimen and detector both move by maintaining a $\omega = \theta$ (specular) relationship. In grazing incidence x-ray diffraction scans, only the detector angle, θ , moves, and fixed grazing specimen angles, ω , allow long diagonal x-ray path lengths through the specimens attenuating bulk reflections and enhancing the intensity from the sample surface. The top two curves, obtained at specimen tilts $\omega = 2^\circ$ and $\omega = 5^\circ$ show enhanced surface layer, zinc oxide, and copper, compared to the normal x-ray diffraction scan in the third curve. The data demonstrated that zinc oxide and copper existed as a thin layer or chunks on top of the tantalum coating. Grazing specimen tilts, however, caused defocusing in the Bragg-Brentano geometry, and broadened diffraction peaks.

Figure 2c shows the x-ray diffraction scans of the four axial specimens after mild etching using sulfuric acid heated to 100°C to remove surface firing debris. The figure shows all surface α -phase with no significant β -tantalum in all four sections, and minute residual zinc oxide and copper firing debris in section 4. Differential etching rates, however, caused slight modification of relative intensities in the tantalum reflections.

Surface Texture and Anisotropy

Two-dimensional x-ray diffraction using a digital image plate obtained at multiple specimen Φ -tilts facilitates fast texture and anisotropy analysis (ref 12). The electronic equivalent, an area detector from Bruker Advanced X-Ray Solutions, was locally interfaced to the Scintag diffractometer for this purpose. Figures 3a through 3d show the x-ray diffraction images of the groove areas for the four axial specimens after etching to remove surface debris. X-rays were focused using 1-mm collimators 105-mm apart to reduce beam divergence. Predominate α -phase tantalum was observed in all four sections. Uniform intensity in the Debye rings further suggested the near-randomness of α -tantalum, and no significant thermal-mechanical property anisotropy. Intensity asymmetry in Figures 3a and 3b is likely due to specimen misalignment, which is difficult for the rifling and curved bore surface geometry. Figure 3c reveals large grain size copper crystallites. Figure 3d shows near-random tantalum (110) and (200) reflections and weak residual copper and zinc oxide reflections from the firing debris. Most importantly, the figure also shows textured β -tantalum (002) in the groove area.

Surface Chemical Composition

Wavelength dispersive x-ray fluorescence for the four axial specimen surfaces showed tantalum, zinc, copper, sulfur, iron, carbon, and oxygen before etching. After etching, tantalum, iron, sulfur, and carbon were observed, and zinc, copper, and oxygen were observed with reduced intensities. The sulfur content is likely a residue from propellant additives such as K_2SO_4 , and the steel content is due to coating loss through liftoff, and/or wear exposing the steel substrate. For a specimen cut from the muzzle end, wavelength dispersive x-ray fluorescence showed weight percentage zinc/tantalum = 0.97 before etching, and 0.05 after etching, and iron/tantalum = 0.20 was unchanged with etching. Firing debris concentrations are expected to increase toward the muzzle end due to a higher velocity of projectiles and gas flow in that region. For the four axial specimens after etching, slight increases in residual zinc, copper, sulfur, oxygen, and carbon concentrations toward the muzzle end were observed.

Hardness

Hardness measurements made using Knoop indentors on a Leitz metallography hardness tester were consistent throughout the coating. They gave ~ 388 KHN₁₀₀, 394 KHN₃₀₀ in α -tantalum areas, ~ 1384 KHN₁₀₀ in β -tantalum areas, ~ 385 KHN₁₀₀, 394 KHN₃₀₀ in steel substrate, and 746 KHN₃₀₀ in the chromium outer interface jacket.

Residual Stress

Surface residual stress distribution in tantalum along the axial direction was measured in the four axial sections before tube sectioning by cutting an axial slit to expose the liner surface. The data are summarized in Table 1. Longitudinal stress was determined using x-ray $\sin^2\phi$ technique, using the tantalum (220) reflection at $2\theta = 157.13^\circ$, and chromium K_α radiation. Elastic constant ($S_2 = (1 + \nu)/E = 7.18 \times 10^{-4} \text{ MPa}^{-1}$) was used for strain-stress conversion, where

γ and E are, respectively, Poisson's ratio and Young's modulus. Compressive surface residual stresses were greater at the breech and the muzzle ends, compared to the middle of the liner. The observed stress distribution reflects the superposition of the compressive atomic peening stresses generated during deposition and the tensile operation stresses generated during the firing operation.

Photomicrograph Analysis

Photomicrographs reveal the color and texture differences brought out by polishing. The harder β -phase tantalum appears lighter in color, whereas softer α -phase tantalum appears darker. Some specimens were etched in 60% sulfuric acid and 40% hydrogen fluoride mix, diluted to 50% distilled water to better reveal the microstructure.

Photomicrograph results for the four axial sections are summarized in Table 1. Photomicrographs of the four sections from breech to muzzle are illustrated in Figures 4a through 4d. The four sections were consistent, showing a thin (~ 3 to $6\ \mu\text{m}$), finger-like growth layer of β -tantalum at the interface, predominately α -tantalum (~ 40 to $50\ \mu\text{m}$) in coating bulk, and trace of β -tantalum on the thin (~ 3 to $5\ \mu\text{m}$) specimen surface. Coating thickness measurements gave 52, 51, 45, and 42 to $45\ \mu\text{m}$ in the four axial specimens from the breech to the muzzle end. The slight decrease in coating thickness toward the muzzle end could be attributed to increased wear toward the muzzle end, or could be attributed to deposition rate. Estimated percentage β/α -concentration increased from 2% to 7% from sections 1 to 4. Higher impurity levels may exist at lower areas in the sputter apparatus, which might have an effect on the higher β -concentration toward the muzzle end.

The muzzle-end specimen is most interesting. Asymmetric coating thickness of 32 to $47\ \mu\text{m}$ at 0° , and 93 to $150\ \mu\text{m}$ at 180° on the circumference were observed. This was most likely due to inappropriate centering of the target, and needs to be corrected. Other potential contributions to thickness variation include pressure differentials at pumping port (near muzzle end) and plasma intensity deviations. Furthermore, drastically different β/α -contents were observed around the tube. On the 180° side, the coatings consisted of predominately α -phase tantalum with few cracks. On the 0° side, the coating showed many cracks, β -tantalum extending from the interface, bulk, to coating surface, and β/α -contents up to 40 to 50% in certain areas. This phase deviation is mostly likely related to sputter energetics, plasma density, sputter rate, and gas pressure in the two regions. Figure 4e shows an example of dense α -tantalum ($105\ \mu\text{m}$ -thick) with excellent adhesion from the muzzle end (180°). Figure 4f depicts an example of a $40\text{-}\mu\text{m}$ thick coating with β -phase nucleation and mixed α - and β -phase growth, high β/α -phase concentration, and vertical and horizontal cracks due to shear stresses. The specimen was obtained from the muzzle end (0°).

The overall land and groove areas were also examined. Generally, good cohesion and adhesion were observed in α -phase tantalum areas, with cracks and disbonding occurring more frequently in β -phase areas. Coating loss was observed to occur in land/groove transition and in land areas, but less in groove areas. Figure 5a shows generally good tantalum coating and substrate conditions after 1500 rounds of firing. Figure 5b shows the land/groove transition zone, with a piece of copper adhering to the left side of the land. The transition zones are more prone to cracks due to the oblique incidence angles of the incoming energetic particle flux during deposition, and higher operation pressure and friction due to the rotation band, especially the side facing the projectile. Figure 5c depicts an expanded view of coating loss in the land/groove transition area, revealing a large crack near the tantalum/steel interface causing coating disbonding, allowing penetration of aggressive propellant gases, and new crack growth in β -tantalum and substrate.

Near the breech end, where there is no or extremely thin coating, severe damage to substrate steel was observed. Figure 6a shows cracks in bare steel induced in the direction of high-friction sliding of the projectiles. Figure 6b illustrates firing damages to bare steel, showing ferrites, untempered martensite, and gray and white layers in the heat-affected zones. The heat-affected zones and environmental-assisted damages warrant further studies. Ahmad *et al.* (ref 3) discussed white layers (fine-grained enriched austenite), and Cote *et al.* (ref 13) described similar gray layers (FeS and FeO) in after-fired chromium-coated steel tubes.

DISCUSSION

Tantalum Phases

The reasons for β -phase formation have been controversial. Numerous authors have reported effects of impurity levels, oxygen and nitrogen concentrations, substrate temperature, substrate type, sputtering gas species, deposition rate, and bias on tantalum phase formation. Ino *et al.* (ref 14), and Roy *et al.* (ref 15) related the role of bombardment energy of atoms and ions to the phase selection of sputtered tantalum films. In this work, the added effects due to asymmetric target centering, pressure differentials, plasma non-uniformity, target-substrate distance, and impurity levels may play a role.

It is common to observe β -phase nucleation and α -phase growth in sputter deposition of tantalum coatings and thin films. Colgan *et al.* (ref 16) reported that a thin layer of interface (tantalum, nitrogen) enhances the growth of α -tantalum. Matson *et al.* (ref 11) suggested that improved ion cleaning of the substrate onto a shutter or "catcher" rather than directly onto the tantalum target, heavier gas species, and higher substrate temperature promote growth of the α -phase. Ino *et al.* (ref 14) and Matson *et al.* (ref 17) further suggested appropriate bias voltage and ion mobility to promote the growth of dense α -phase. Interface layers, such as niobium, have also been shown to promote nucleation in α -phase tantalum (refs 9, 10, 18); interface layers still hold great promise for the minimization and elimination of interface β -phase tantalum.

Residual Stress

Thornton is well known for his life-long work on physical vapor deposition (ref 19), including residual stress. Windischmann (ref 20) summarized experimental and modeling investigations of intrinsic stress in sputtering deposition. Very high residual stresses of the order -2.5 GPa to 2.0 GPa in as-deposited tantalum films have been reported. Clevenger *et al.* (ref 21) studied stress relaxation in tantalum β - to α -phase transformation. Cabral *et al.* (ref 22) reported thermal cycling increases the compressive stresses to produce very fragile films. Horizontal and vertical cracks have commonly been observed in as-deposited tantalum films, near the interface and in buried β - to α -transition areas. Highly stressed β -phase tantalum is believed to be the major cause of cracks and coating loss.

Microstructure

Due to the fact that high-temperature deposition can deplete favorable residual stress distributions induced by swage autofrettage, coating deposition temperature is generally limited to <500°C. Thornton's structure zone model suggests zone 1 represents tapered narrow crystal growth with substantial voiding, and zone T represents dense fibrous grain growth. Dense and fine-grained zone-T microstructure was observed in the fired tantalum coating.

Surface Firing Debris

Zinc oxide was generated due to the interaction of the projectile gilding metal (95% copper and 5% zinc) in the rotating band riding on the rifling of the tube. Zinc phosphate is used in the phosphate process to enhance corrosion resistance and paint adhesion of the projectiles. In addition, 20-mm projectiles are made of cartridge brass (70% copper and 30% zinc). Zinc and copper are believed to also exist in electrolytic chromium-coated cylinders after firing, and are not expected to affect the accuracy and effectiveness of the tube operation.

CONCLUSIONS

1. X-ray diffraction showed the growth front of the liner, in closest contact with the projectiles, was predominately body-centered-cubic α -phase tantalum. Soft, ductile, and chemical resistant α -phase tantalum contributed to the success of the coatings.
2. Photomicrographs showed a thin layer of β -phase nucleation, α - or mixed α - and β -tantalum grain growth. The α -phase exhibited excellent cohesion and adhesion; cracks, disbonding, and liftoff occurred mostly in brittle β -tantalum areas.

3. Coating loss was observed most frequently in land/groove transition and land areas, and less in the groove areas.
4. A thin layer of zinc oxide and copper firing debris were observed. The firing debris resulted from the gas/projectile interaction, and is not expected to affect the accuracy and operation of the tube.
5. In the breech end where no coating was deposited, extensive cracking and heat damage to steel was observed. This demonstrated the effectiveness of tantalum as protection against high-temperature wear and erosion.
6. Suggested coating optimization includes minimization and elimination of β -phase tantalum, improved subsurface residual stress and density/porosity monitoring and control, and correction for centering of target to produce a more uniform coating.

REFERENCES

1. Cullinan, R.L., D'Andrea, G., Croteau, P., and Arnold, C., U.S. Army Technical Report ARLCB-TR-80027, Benet Laboratories, Watervliet, NY, December 1980.
2. Ahmad, I., Barranco, J., Aalto, P., and Cox, J., U.S. Army Technical Report ARLCB-TR-83029, Benet Laboratories, Watervliet, NY, September 1983.
3. Ahmad, I., *Gun Propulsion Technology*, (Ludwig Stiefel, Ed.), Vol. 109, Progress in Astronautics and Aeronautics Series, AIAA, Washington, DC, 1988, pp. 311-355.
4. Vasilakis, J., "Strategic Environmental Research and Development Program (SERDP) - Tri-Service Green Gun Barrel Project, Year-End Report," Benet Laboratories, Watervliet, NY, 2001.
5. Cullinan, R.L., D'Andrea, G., and Croteau, P., U.S. Army Technical Report ARLCB-TR-81011, Benet Laboratories, Watervliet, NY, April 1981.
6. Ahmad, I., Spiak, W.A., and Janz, G.J., *Journal of Applied Electrochemistry*, Vol. 11, No. 3, 1981, p. 291.
7. Lee, S.L., Cipollo, M., Windover, D., and Rickard, C., *Surface and Coatings Technology*, Vol. 120-121, 1999, p. 44.
8. Cox, J.F., and McClanahan, E.D., in: *Proceedings of Tri-Service Gun Tube Wear and Erosion Symposium*, 1982, p. 277.
9. Matson, D.W., Merz, M.D., and McClanahan, E.D., *Journal of Vacuum Science and Technology A*, Vol. 10, No. 4, 1992, p. 1791.
10. Lee, S.L., and Windover, D., *Surface and Coatings Technology*, Vol. 108-109, 1998, p. 65.
11. Matson, D.W., McClanahan, E.D., Rice, J.P., Lee, S.L., and Windover, D., *Surface and Coatings Technology*, Vol. 133-134, 2000, p. 411.
12. Lee, S.L., Windover, D., Doxbeck, M., Nielsen, M., Kumar, A., and Lu, T.-M., *Thin Solid Films*, Vol. 377-378, 2000, p. 447.
13. Cote, P.J., and Rickard, C., *Wear*, Vol. 241, 2000, p. 17.
14. Ino, K., Shinohara, T., Ushikai, T., and Ohmi, T., *Journal of Vacuum Science and Technology A*, Vol. 15, 1997, p. 2627.
15. Roy, R.A., Catania, P., Saenger, K.L., Cuomo, J.J., and Lossy, R.L., *Journal of Vacuum Science and Technology B*, Vol. 11, No. 5, September/October 1993, p. 1921.

16. Colgan, E.G., and Fryer, P.M., U.S. Patent No. WO92/07968, IBM Corporation, 1992.
17. Matson, D.W., McClanahan, E.D., Lee, S.L., and Windover, D., *Surface and Coatings Technology*, to be published.
18. Face, D.W., and Prober, D.E., *Journal of Vacuum Science and Technology A*, Vol. 5, 1987, p. 3408.
19. Thornton, J.A., "Physical Vapor Deposition," in *Semiconductor Materials and Process Technology Handbook*, (G.E. McGuire, Ed.), Noyes Publications, 1988, p. 329.
20. Windischmann, H., *Critical Reviews in Solid State and Material Sciences*, Vol. 17, 1992, p. 547.
21. Clevenger, L.A., Mutscheller, A., Harper, J.M.E., Cabral, C., Jr., and Barmak, K., *Journal of Applied Physics*, Vol. 72, No. 10, 15 November 1992, p. 4918.
22. Cabral, C., Jr., Clevenger, L.A., and Schad, R.G., *Journal of Vacuum Science and Technology B*, Vol. 12, 1994, p. 2818.

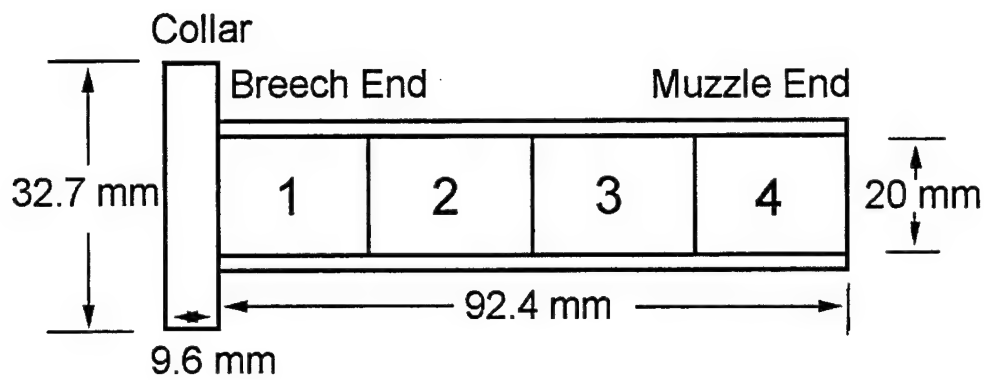


Figure 1a. Liner configuration from breech to muzzle end.
The four sections are marked to facilitate data acquisition and analysis.

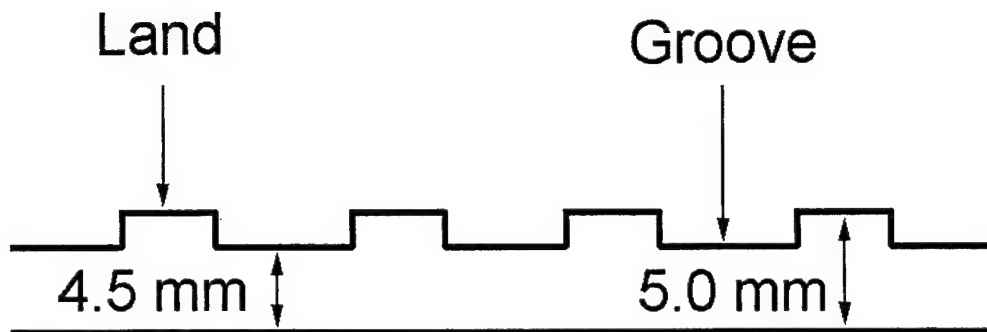


Figure 1b. Land and groove geometry in a rifled tube.

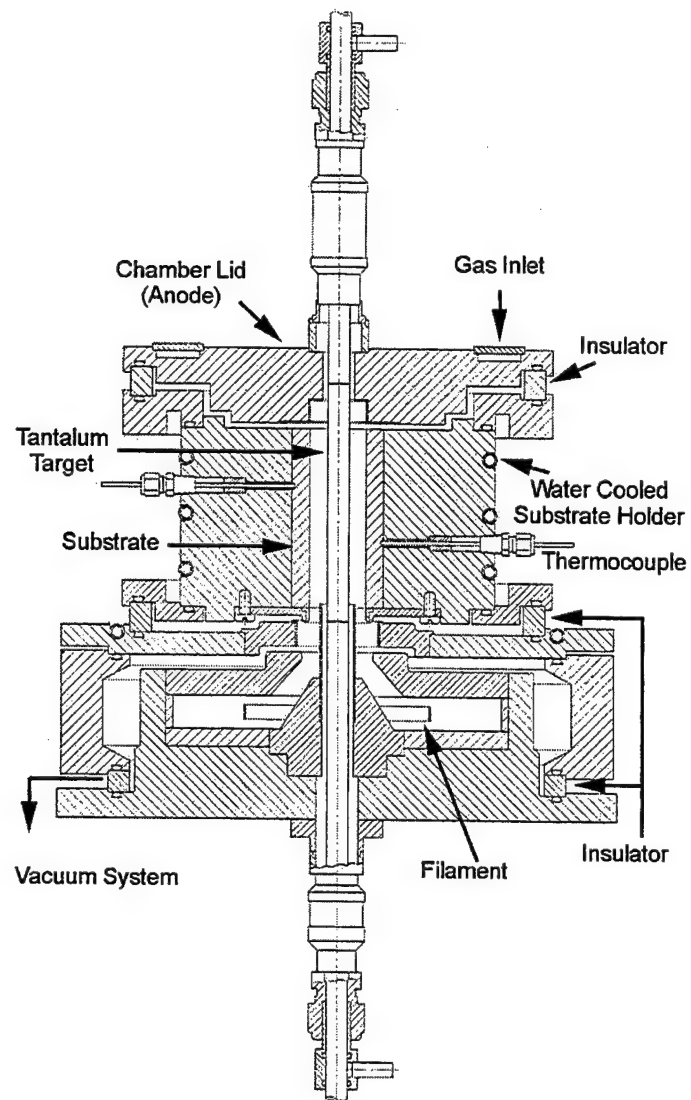


Figure 1c. Triode-sputter apparatus at Pacific Northwest National Laboratory.

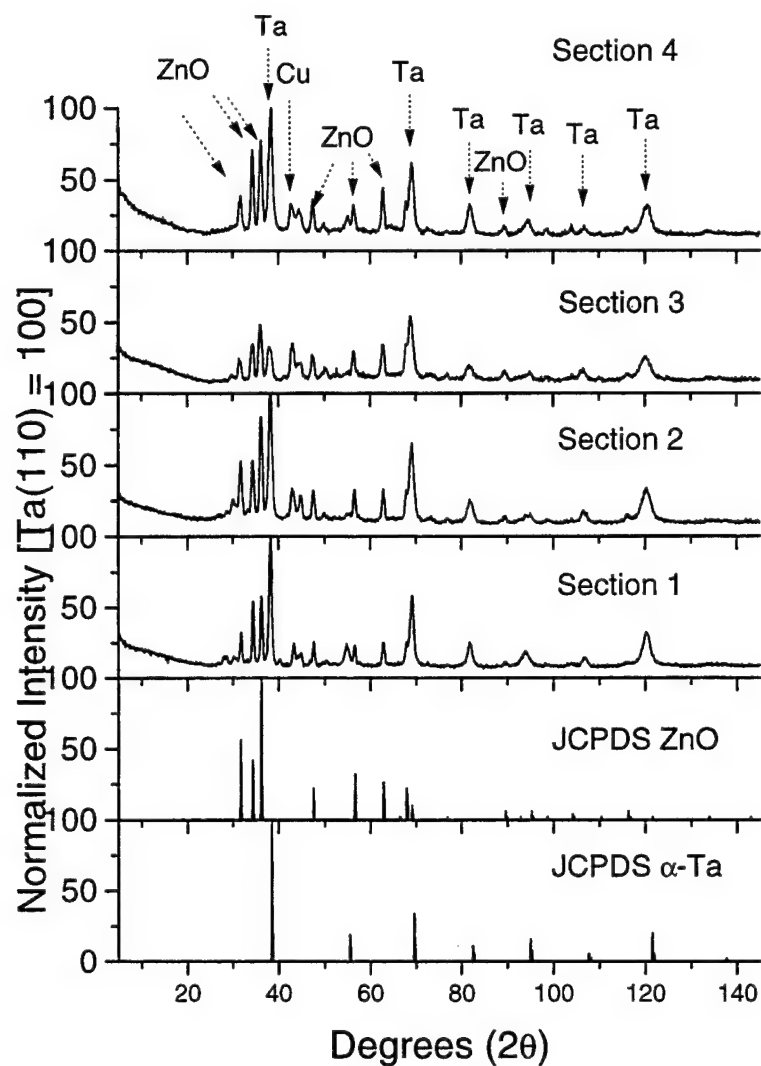


Figure 2a. Growth surface x-ray diffraction from breech to muzzle end (sections 1 through 4), showing surface α -phase tantalum, and oxide and copper firing debris.

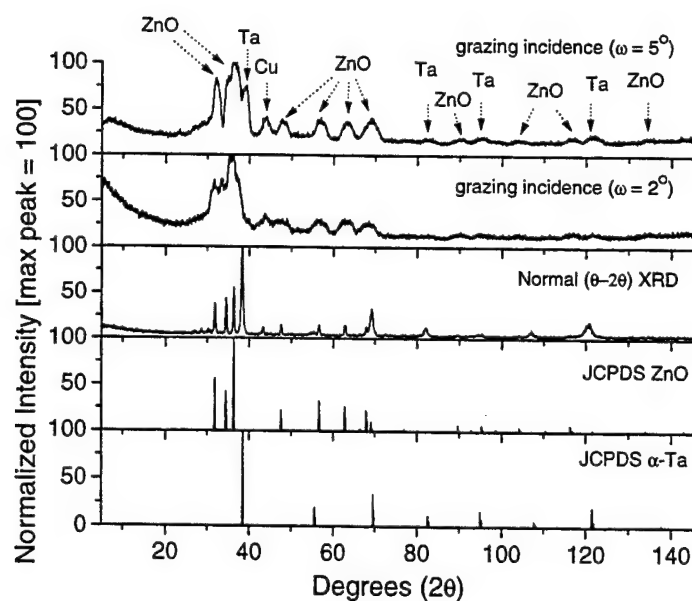


Figure 2b. Grazing incidence x-ray diffraction at $\omega = 5^\circ$ and $\omega = 2^\circ$ compared to conventional x-ray diffraction, demonstrating that the observed zinc oxide and copper are on the surface of sputtered tantalum coating.

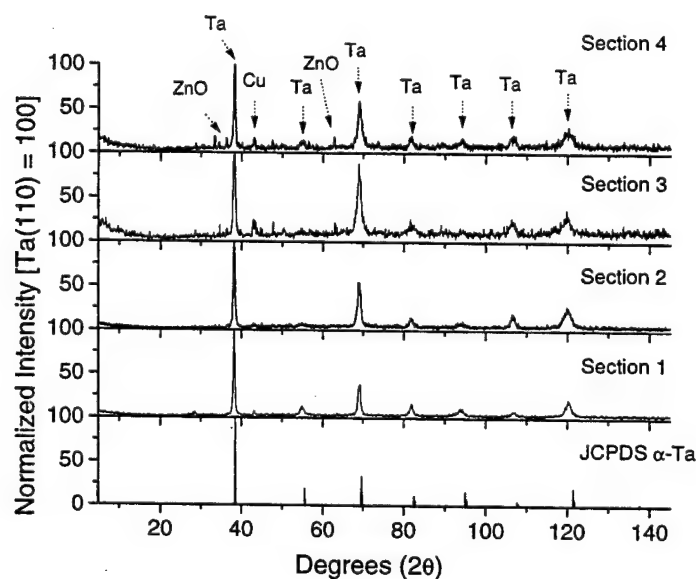


Figure 2c. Growth surface x-ray diffraction after etching to remove surface firing debris, showing all α -phase tantalum, residual zinc oxide and copper, and minor relative intensity change due to differential etching.

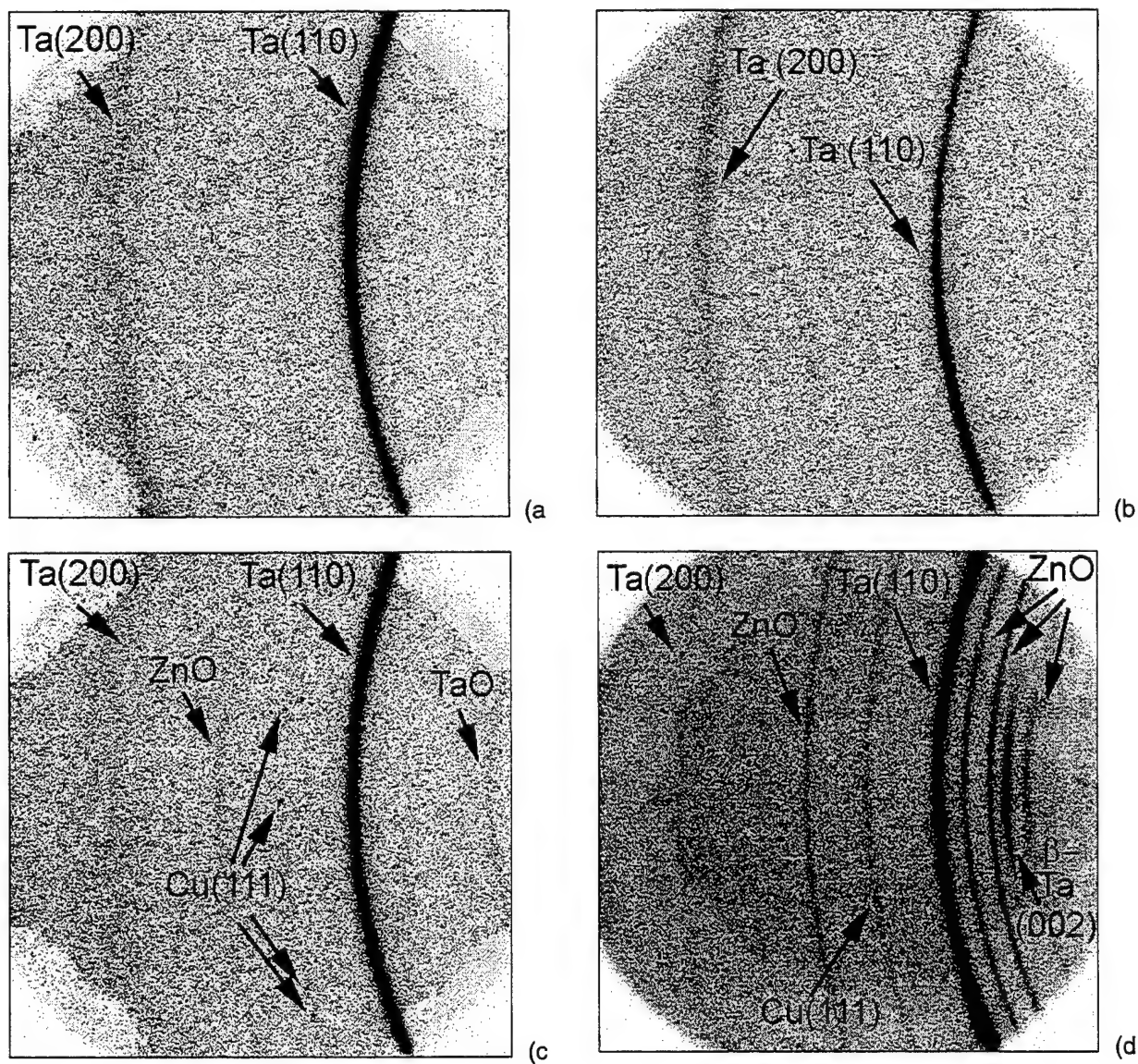


Figure 3. Two-dimensional area detector images of groove areas of the four sections after etching. Figures 3a through d show near-random α -phase tantalum and weak copper and zinc oxide reflections. Figure 3c also shows large copper crystallites. Figure 3d shows additional weak textured β -phase tantalum with preferred (002) orientation.

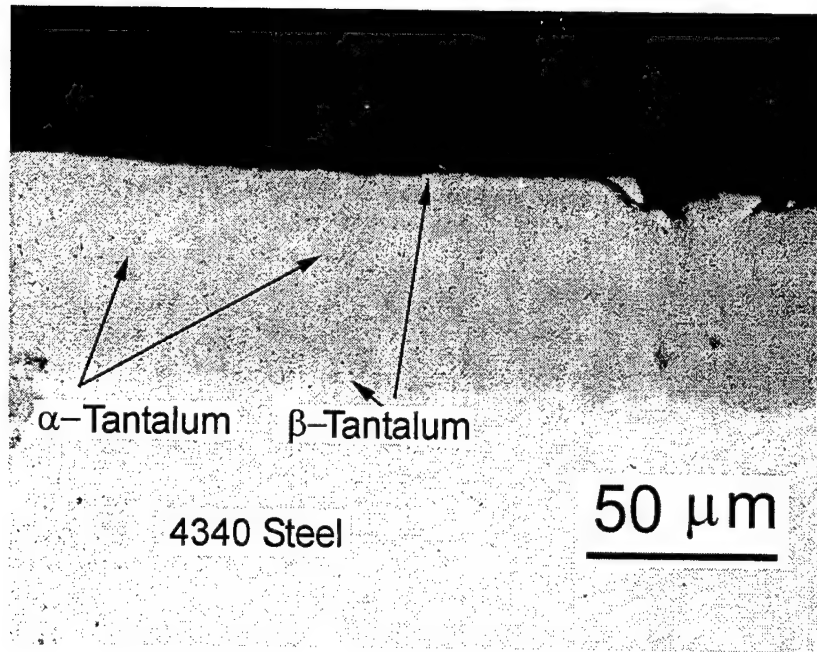


Figure 4a. Photomicrograph of specimen cut from section #1 of the liner.

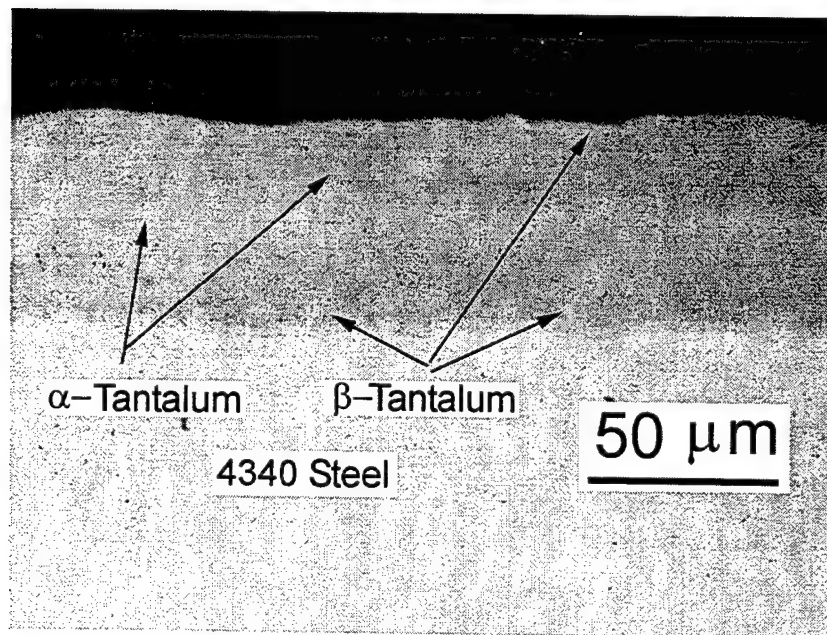


Figure 4b. Photomicrograph of specimen cut from section #2 of the liner.

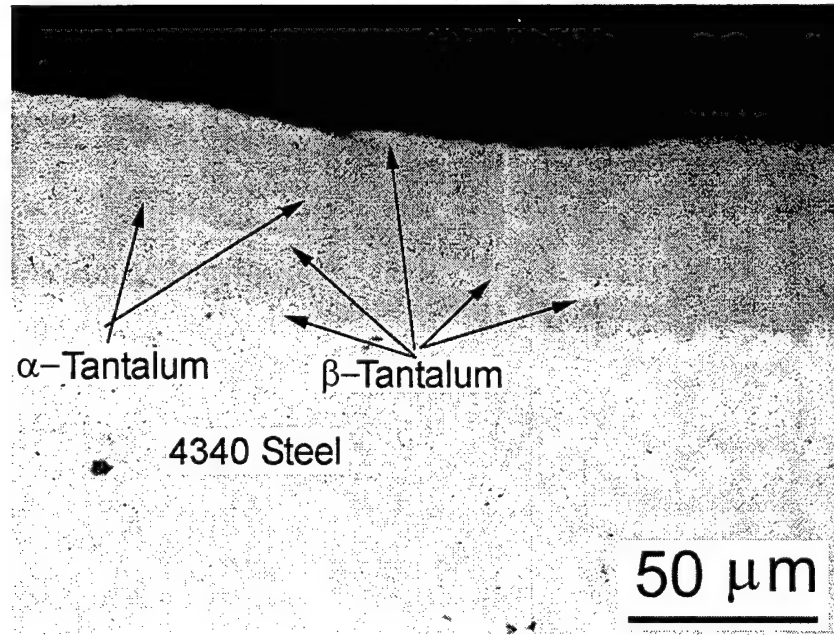


Figure 4c. Photomicrograph of specimen cut from section #3 of the liner.

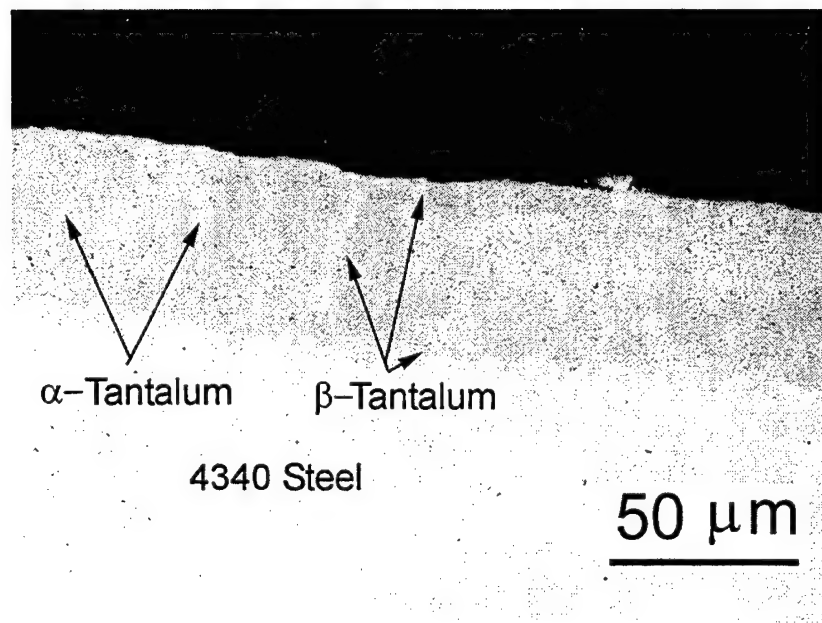


Figure 4d. Photomicrograph of specimen from section #4 of the liner.

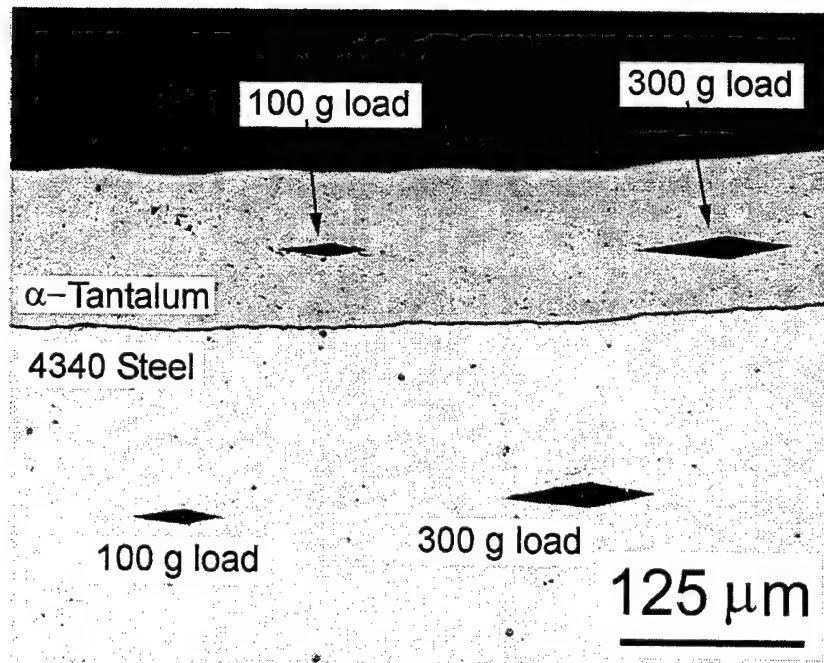


Figure 4e. Single-phase α -tantalum with good cohesion and adhesion to the 4340 steel substrate.

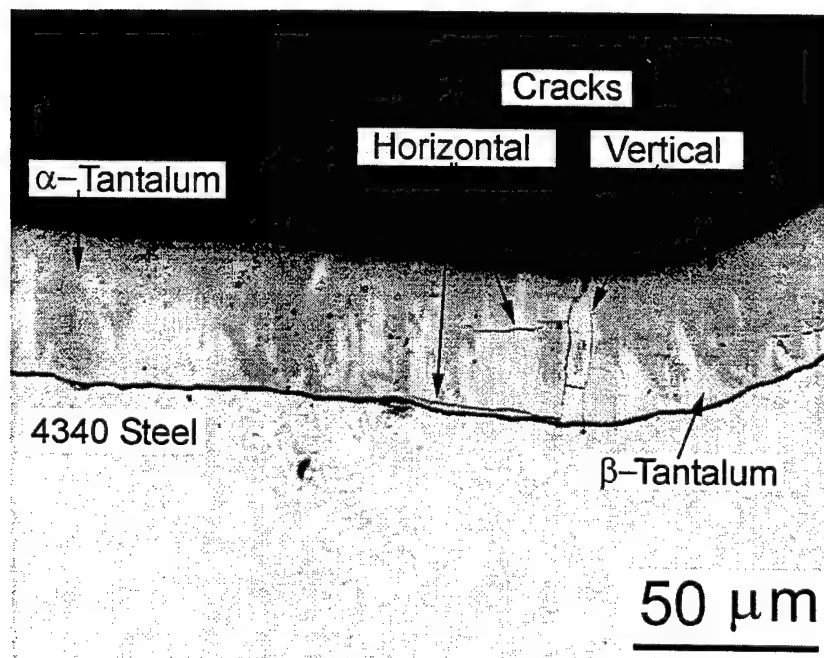


Figure 4f. Coating with β -phase tantalum nucleation and mixed α - and β -growth, showing horizontal and vertical cracks in the β -tantalum region.

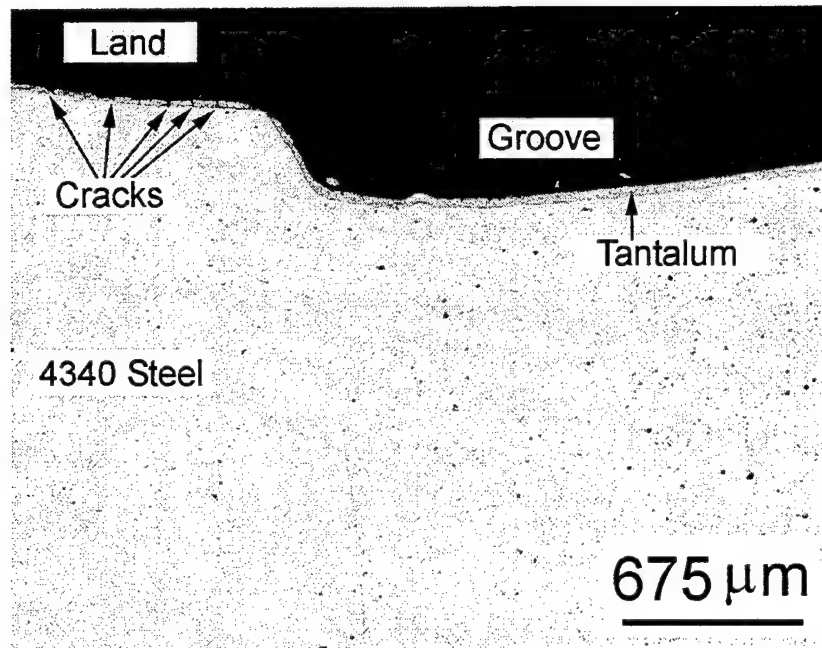


Figure 5a. Land/groove area of sputtered tantalum coating on steel after firing 1500 rounds

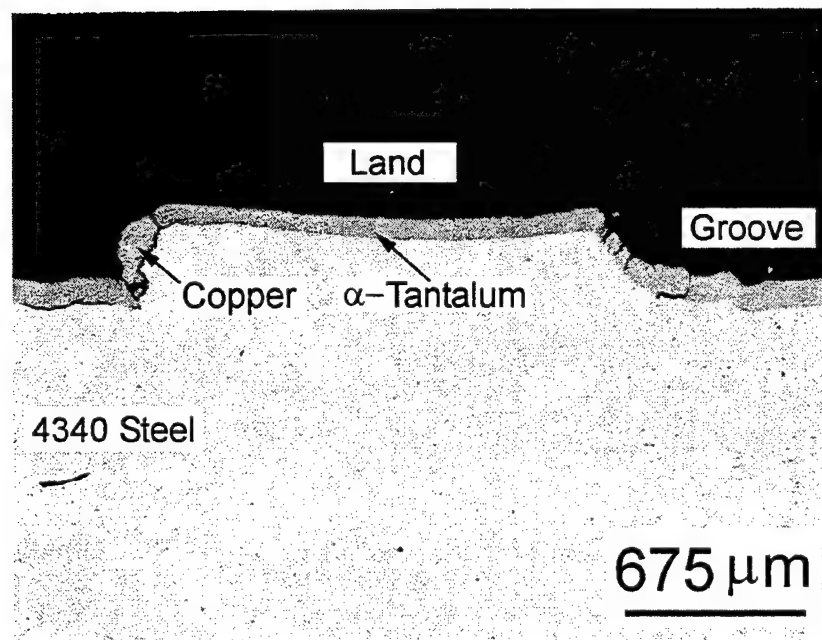


Figure 5b. Typical cracks in the land/groove transition area, showing a piece of copper on the left arm of the land/groove transition area.

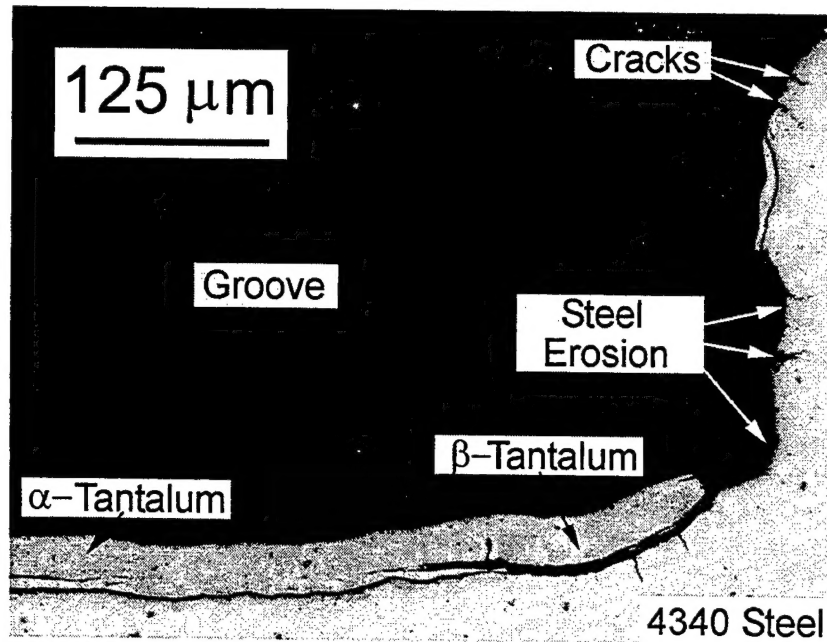


Figure 5c. Coating loss in the land/groove transition area, revealing large crack near tantalum/steel interface. Note that in the cracked groove area, penetration of propellant gases enhanced crack growth in steel and in β -tantalum.

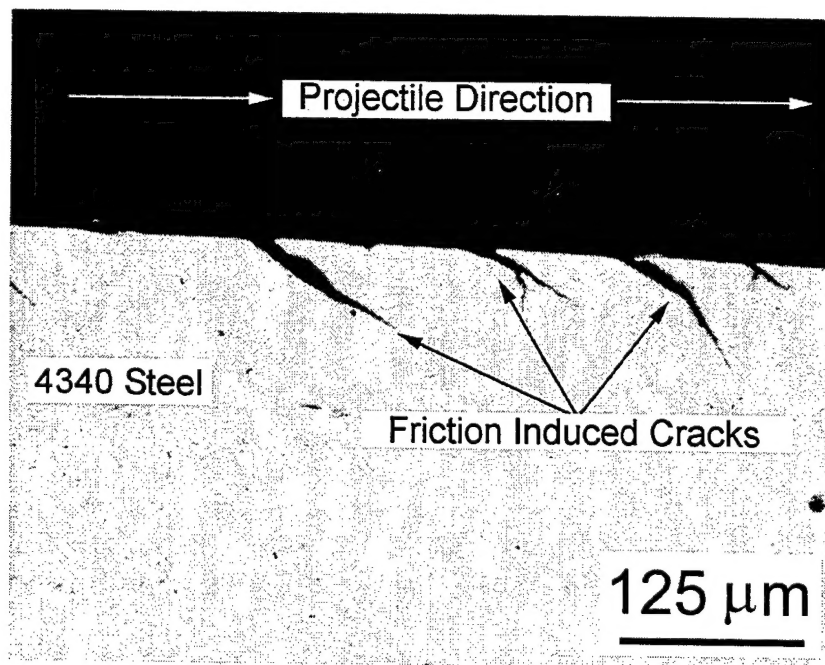


Figure 6a. Cracks in bare steel in the direction of high-friction sliding due to projectile motion, in areas with no sputtered tantalum (unetched).

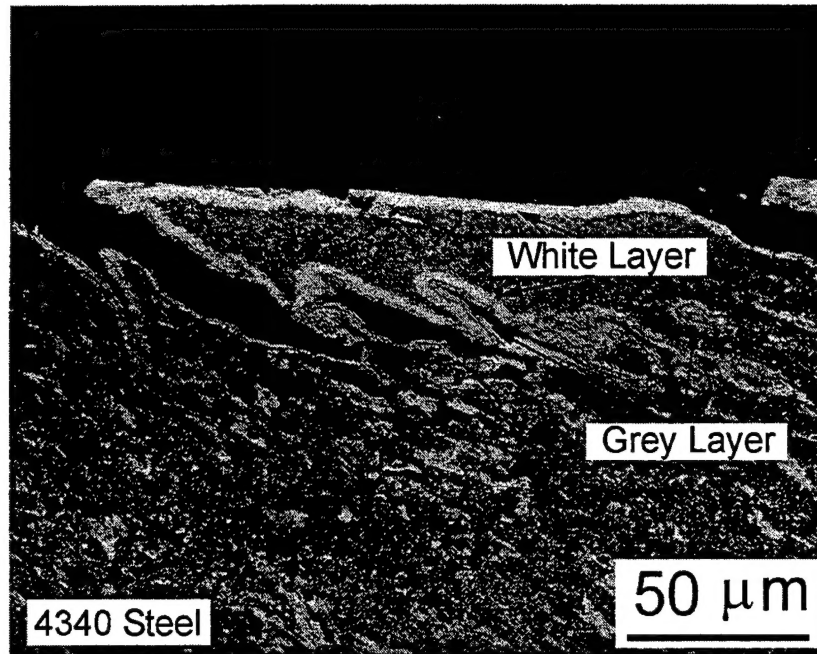


Figure 6b. Environmental-assisted heat damages in steel forming white and gray layers in areas with no sputtered tantalum (etched).

TECHNICAL REPORT INTERNAL DISTRIBUTION LIST

	<u>NO. OF COPIES</u>
TECHNICAL LIBRARY ATTN: AMSTA-AR-CCB-O	5
TECHNICAL PUBLICATIONS & EDITING SECTION ATTN: AMSTA-AR-CCB-O	3
OPERATIONS DIRECTORATE ATTN: SIOWV-ODP-P	1
DIRECTOR, PROCUREMENT & CONTRACTING DIRECTORATE ATTN: SIOWV-PP	1
DIRECTOR, PRODUCT ASSURANCE & TEST DIRECTORATE ATTN: SIOWV-QA	1

NOTE: PLEASE NOTIFY DIRECTOR, BENÉT LABORATORIES, ATTN: AMSTA-AR-CCB-O OF ADDRESS CHANGES.

TECHNICAL REPORT EXTERNAL DISTRIBUTION LIST

	<u>NO. OF COPIES</u>		<u>NO. OF COPIES</u>
DEFENSE TECHNICAL INFO CENTER		COMMANDER	
ATTN: DTIC-OCA (ACQUISITIONS)	2	ROCK ISLAND ARSENAL	
8725 JOHN J. KINGMAN ROAD		ATTN: SIORI-SEM-L	1
STE 0944		ROCK ISLAND, IL 61299-5001	
FT. BELVOIR, VA 22060-6218			
COMMANDER		COMMANDER	
U.S. ARMY ARDEC		U.S. ARMY TANK-AUTMV R&D COMMAND	
ATTN: AMSTA-AR-WEE, BLDG. 3022	1	ATTN: AMSTA-DDL (TECH LIBRARY)	1
AMSTA-AR-AET-O, BLDG. 183	1	WARREN, MI 48397-5000	
AMSTA-AR-FSA, BLDG. 61	1	COMMANDER	
AMSTA-AR-FSX	1	U.S. MILITARY ACADEMY	
AMSTA-AR-FSA-M, BLDG. 61 SO	1	ATTN: DEPT OF CIVIL & MECH ENGR	1
AMSTA-AR-WEL-TL, BLDG. 59	2	WEST POINT, NY 10966-1792	
PICATINNY ARSENAL, NJ 07806-5000			
DIRECTOR		U.S. ARMY AVIATION AND MISSILE COM	
U.S. ARMY RESEARCH LABORATORY		REDSTONE SCIENTIFIC INFO CENTER	2
ATTN: AMSRL-DD-T, BLDG. 305	1	ATTN: AMSAM-RD-OB-R (DOCUMENTS)	
ABERDEEN PROVING GROUND, MD		REDSTONE ARSENAL, AL 35898-5000	
21005-5066			
DIRECTOR		COMMANDER	
U.S. ARMY RESEARCH LABORATORY		U.S. ARMY FOREIGN SCI & TECH CENTER	
ATTN: AMSRL-WM-MB (DR. B. BURNS)	1	ATTN: DRXST-SD	1
ABERDEEN PROVING GROUND, MD		220 7TH STREET, N.E.	
21005-5066		CHARLOTTESVILLE, VA 22901	
COMMANDER			
U.S. ARMY RESEARCH OFFICE			
ATTN: TECHNICAL LIBRARIAN	1		
P.O. BOX 12211			
4300 S. MIAMI BOULEVARD			
RESEARCH TRIANGLE PARK, NC 27709-2211			

NOTE: PLEASE NOTIFY COMMANDER, ARMAMENT RESEARCH, DEVELOPMENT, AND ENGINEERING CENTER,
BENET LABORATORIES, CCAC, U.S. ARMY TANK-AUTOMOTIVE AND ARMAMENTS COMMAND,
AMSTA-AR-CCB-O, WATERVLIET, NY 12189-4050 OF ADDRESS CHANGES.
